



UNIVERSITY OF LEEDS

This is a repository copy of *Designing strain-balanced GaN/AlGaIn quantum well structures: Application to intersubband devices at 1.3 and 1.55 μm wavelengths* .

White Rose Research Online URL for this paper:
<http://eprints.whiterose.ac.uk/1690/>

Article:

Jovanovic, V.D., Ikonc, Z., Indjin, D. et al. (3 more authors) (2003) Designing strain-balanced GaN/AlGaIn quantum well structures: Application to intersubband devices at 1.3 and 1.55 μm wavelengths. *Journal of Applied Physics*, 93 (6). pp. 3194-3197. ISSN 1089-7550

<https://doi.org/10.1063/1.1556177>

Reuse

See Attached

Takedown

If you consider content in White Rose Research Online to be in breach of UK law, please notify us by emailing eprints@whiterose.ac.uk including the URL of the record and the reason for the withdrawal request.



eprints@whiterose.ac.uk
<https://eprints.whiterose.ac.uk/>

Designing strain-balanced GaN/AlGaIn quantum well structures: Application to intersubband devices at 1.3 and 1.55 μm wavelengths

V. D. Jovanović,^{a)} Z. Ikonić, D. Indjin, and P. Harrison
School of Electronic and Electrical Engineering, University of Leeds, Leeds LS2 9JT, United Kingdom

V. Milanović
School of Electrical Engineering, Bulevar Kralja Aleksandra 73, 11120 Belgrade, Yugoslavia

R. A. Soref
Sensor Directorate, Air Force Research Laboratory, AFRL/SNHC, Hanscom Air Force Base, Massachusetts 01731

(Received 3 December 2002; accepted 8 January 2003)

A criterion for strain balancing of wurtzite group-III nitride-based multilayer heterostructures is presented. Single and double strain-balanced GaN/AlGaIn quantum well structures are considered with regard to their potential application in optoelectronic devices working at communication wavelengths. The results for realizable, strain-balanced structures are presented in the form of design diagrams that give both the intersubband transition energies and the dipole matrix elements in terms of the structural parameters. The optimal parameters for structures operating at $\lambda \sim 1.3$ and $1.55 \mu\text{m}$ were extracted and a basic proposal is given for a three level intersubband laser system emitting at $1.55 \mu\text{m}$ and depopulating via resonant longitudinal optical (LO) phonons ($\hbar\omega_{\text{LO}} \approx 90 \text{ meV}$). © 2003 American Institute of Physics. [DOI: 10.1063/1.1556177]

I. INTRODUCTION

In recent years intersubband transitions (ISBTs) in AlGaIn-based heterostructures have emerged as a promising route for access to the near-infrared spectral range, while also showing ultrafast carrier dynamics. A few groups have reported intersubband absorption for wavelengths around 1.3 and $1.55 \mu\text{m}$,¹⁻⁷ that are important for optoelectronic telecommunications, as well as ultrashort relaxation times $\tau_{\text{rel}} \sim \text{fs}$ in quantum well structures and superlattices.⁸⁻¹⁰ These experimental successes suggest possible application in quantum well infrared photodetectors (QWIPs), optical switches or even intersubband lasers. Improvements in the molecular beam epitaxy growth technique that allow control of layer widths of the order of a few monolayers make feasible the design and growth of complex structures. However, growth of uniform, dislocation-free multilayer, optically thick stacks is still a considerable challenge.^{11,12} To achieve pseudomorphic growth, there is the requirement of strain balance upon the whole structure. Although multilayer structures generally show much better stability against relaxation than do homogeneous strained layers, one should still aim at achieving full strain balance when designing such a structure in order to have reliable, reproducible growth.

Several approaches to the design of strain-balanced structures have been considered,¹³ but they were usually restricted to two-layer structures (e.g., single quantum wells) based upon semiconductor materials with cubic symmetry. In this article we extend the “zero-strain” approach¹³ to multilayer structures based upon wurtzite (e.g., GaN/AlIn) semiconductors grown in the conventional [0001] direction,

and then we present design diagrams oriented their possible application in optoelectronics.

II. THEORETICAL CONSIDERATIONS

The zero-strain condition¹³ is the only theoretical approach that accounts for different elastic constants of layers, in contrast to the more common average lattice or thickness weighted methods.¹⁴ It is based on minimizing the average elastic energy for the whole multilayer structure, i.e.,

$$\bar{f} = \frac{\sum_{k=1}^n f_k l_k}{\sum_{k=1}^n l_k}, \quad (1)$$

where l_k is the width and f_k strain energy density of the k th layer.

Within the framework of classical elastic theory¹⁵ the elastic energy density of the k th layer is

$$f_k = \sum_{i=1}^6 \sum_{j=1}^6 \frac{1}{2} c_{ij}^{(k)} \epsilon_i^{(k)} \epsilon_j^{(k)}, \quad (2)$$

where $c_{ij}^{(k)}$ is the elastic tensor element and $\epsilon_{i,j}^{(k)}$ the strain tensor element for a hexagonal crystallographic system in matrix notation¹⁵ of the k th layer.

Since we consider a wurtzite based multilayer system grown along the [0001] axis, the corresponding stress tensor element (σ_3) should equal zero. By using formulas given in Refs. 15 and 16 the biaxial strain tensor has only diagonal elements and is given by

$$\epsilon = \begin{bmatrix} \epsilon_1 & \epsilon_6 & \epsilon_5 \\ \epsilon_6 & \epsilon_1 & \epsilon_4 \\ \epsilon_5 & \epsilon_4 & \epsilon_3 \end{bmatrix} = \begin{bmatrix} \epsilon_1 & 0 & 0 \\ 0 & \epsilon_1 & 0 \\ 0 & 0 & -2 \frac{c_{13}}{c_{33}} \epsilon_1 \end{bmatrix}, \quad (3)$$

^{a)}Electronic mail: eenvj@leeds.ac.uk

where $\epsilon_1 = (a - a_0)/a_0$ is the in-plane strain, a is the buffer in-plane lattice constant (along the wurtzite a axis) and a_0 is the lattice constant of a layer in strain-free conditions. From Eqs. (2) and (3) it follows that the strain energy density in a layer is

$$f_k = A_k \cdot [\epsilon_1^{(k)}]^2, \quad (4)$$

where $A = c_{11} + c_{12} - 2c_{13}^2/c_{33}$. Equation (1) may then be written as

$$\bar{f} = \frac{\sum_{k=1}^n A_k [\epsilon_1^{(k)}]^2 l_k}{\sum_{k=1}^n l_k}. \quad (5)$$

The pseudomorphic condition relates the strain in adjacent layers ($\epsilon_1^{(k)}$ and $\epsilon_1^{(k-1)}$) and is given as

$$\epsilon_1^{(k)} = \frac{a_{k-1}}{a_k} \epsilon_1^{(k-1)} + \frac{a_{k-1} - a_k}{a_k}, \quad (6)$$

and the average in-plane stress that follows is

$$\bar{\sigma} = \frac{\partial \bar{f}}{\partial \epsilon_1^{(1)}} = \frac{2}{l_1 + l_2 + l_3 + \dots} \times \left\{ A_1 \epsilon_1^{(1)} l_1 + A_2 \epsilon_1^{(2)} l_2 \frac{\partial \epsilon_1^{(2)}}{\partial \epsilon_1^{(1)}} + A_3 \epsilon_1^{(3)} l_3 \frac{\partial \epsilon_1^{(3)}}{\partial \epsilon_1^{(1)}} + \dots \right\}. \quad (7)$$

The zero-stress (or strain-balance) condition means that the in-plane stress is zero, and using $\partial \epsilon_1^{(k)}/\partial \epsilon_1^{(1)} = a_1/a_k$ ($k = 2, 3, \dots$) Eq. (7) then gives

$$A_1 \epsilon_1^{(1)} l_1 + A_2 \epsilon_1^{(2)} l_2 \frac{a_1}{a_2} + A_3 \epsilon_1^{(3)} l_3 \frac{a_1}{a_3} + \dots = 0, \quad (8)$$

which delivers the buffer lattice constant necessary for the strain-balanced multilayer structure as

$$a_0 = \frac{\sum_{k=1}^n A_k l_k / a_k}{\sum_{k=1}^n A_k l_k / a_k^2}, \quad (9)$$

and, therefore, in case of GaN/AlGaIn structures, the Al content in the buffer follows straightforwardly.

If a multilayer structure has periodicity, the above expression should be understood to apply to n layers that constitute a single period, and the whole structure will then clearly be strain balanced.

The strain level in individual layers directly influences the conduction band profile, due to the large strain-dependent, piezoelectric polarization induced electric field.¹⁷ This means that strain-balanced device design and optimization are more complicated than would be the case with no polarization. This is because any single structural parameter cannot be varied independently (in order to change the sub-band structure), so the strain-balance condition has to be met as well. In the remaining part of this article, we present suitable design diagrams for strain-balanced single and double GaN/AlGaIn QW structures; see Fig. 1. Single QW structures were explored with respect to the ISBT energies and dipole matrix elements corresponding to the $1 \rightarrow 2$ transition with a view towards their possible application in devices like QWIPs or saturable switches. Double QWs were explored

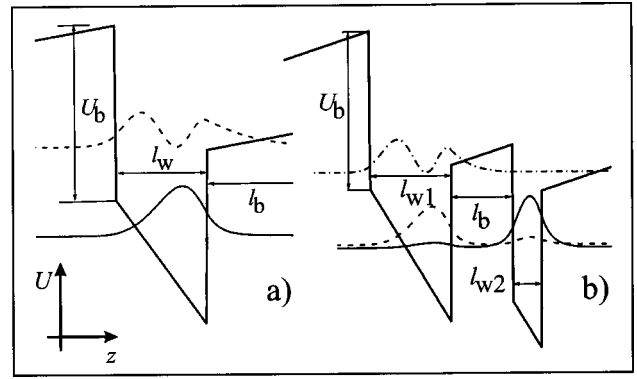


FIG. 1. Conduction band profile and wave function moduli of single and coupled double GaN/AlGaIn QWs, and the notation of structural parameters.

with respect to transition energies between $|1\rangle$ and $|2\rangle$, and $|2\rangle$ and $|3\rangle$, with a view towards their potential application in three-level intersubband lasers.¹⁸

In the calculations we have employed the effective mass model and solved the envelope function Schrödinger equation with bulk nonparabolicity included via the energy dependent effective mass (two band Kane model).¹⁹ Nonlinear piezoelectric and spontaneous polarizations were also included²⁰ and the fields induced were calculated from the simple expression²¹ (all constraints of that approach are satisfied here²²)

$$F_j = \frac{\sum_k (P_k - P_j) l_k / \epsilon_k}{\epsilon_j \sum_k l_k / \epsilon_k}, \quad (10)$$

where $P_i = P_{sp}^i + P_{pz}^i$ is the total polarization given as a sum of piezoelectric and spontaneous (pyroelectric) polarization within a layer of width l_i . In calculating the alloy band gap we have included the effect of bowing.²³

The Schrödinger equation used within this model is

$$-\frac{\hbar^2}{2} \frac{\partial}{\partial z} \left(\frac{1}{m(z, E)} \frac{d\Psi}{dz} \right) + U(z)\Psi = E\Psi, \quad (11)$$

where the position- and energy-dependent effective mass is $m(z, E) = m(z) \{1 + [E - U(z)]/E_g(z)\}$, where $m(z)$, $E_g(z)$ and $U(z)$ denote, respectively, the parabolic effective mass, band gap and conduction band edge (which includes the band edge discontinuities and the polarization-induced potential). All three vary along coordinate z because of modulation of the material composition. This equation may be solved by a standard shooting method, starting with a well-behaved wave function on one side and scanning for energies where it is well behaved on the other side. However, this method loses stability for wider structures, typically with those five wells or so. We have therefore employed a finite-difference method, in which Eq. (11) is written in discretized form, in N_z points along the z axis like, e.g., in Ref. 24, and reduces to a matrix eigenvalue problem, where the Hamiltonian matrix is tridiagonal. However, the energy E appears not only in the main diagonal, but in all the terms (via the effective mass), which leads to a nonlinear eigenvalue problem,

$$[H(E)]\psi = E\psi, \quad (12)$$

which cannot be solved by conventional diagonalization routines that handle linear eigenvalue problems $[H]\psi = E\psi$ (which would be the case if the Hamiltonian, i.e., the effective mass in it, is not energy dependent). In the field of electronic structure calculations nonlinear eigenvalue problems also appear, e.g., in augmented plane wave methods, but the matrix there is not tridiagonal, and the computational demands are considerably larger than for linear eigenproblems, so sophisticated methods have been devised to speed up the process.²⁵ Here, however, we take advantage of the tridiagonal form of the finite-difference representation Eq. (11) for fast solving of Eq. (12). We first scan for energies E_i where

$$\det([H(E_i)] - E_i[I]) = 0 \quad (13)$$

is satisfied [the E_i are obviously the eigenvalues of Eq. (12) and $[I]$ is the $N_z \times N_z$ unity matrix]. Calculation of the determinant of the tridiagonal matrix²⁶ is fast and scales linearly with its size N_z (just as does the shooting method), hence it is easy to achieve high precision. In this particular problem it suffices to find just the sign, not the full value of the determinant, and supply it to the bisection routine, a feature which almost cuts into half the computational time. Normally, one is interested in only a few lowest, rather than all, N_z eigenvalues of Eq. (12).

To find the eigenvectors, i.e., the wave functions, Eq. (12) can be written, for any particular E_i in the form of a fictitious linear eigenproblem,

$$([H(E_i)] - E_i[I])\psi_i = \lambda\psi_i. \quad (14)$$

One of the N_z eigenvalues λ will be (almost, because of roundoff errors) equal to zero, and the eigenvector corresponding to it is actually the eigenvector of Eq. (12) corresponding to eigenenergy E_i [other eigenvalues and eigenvectors of Eq. (14) are physically meaningless]. For this task we use standard diagonalization routines (EISPACK) that allow evaluation of a single, selected eigenvector—that with the already known, zero eigenvalue. Alternatively, upon finding eigenvalues E_i , one may also calculate eigenvectors by solving the tridiagonal system of linear equations corresponding to Eq. (12) using appropriate fast routines,²⁶ but this approach was found to offer somewhat less stability.

The method was found to be about as equally fast and accurate as the shooting method (in cases where both work well), while retaining full stability where the shooting method fails.

The calculated results were used to make contour plots, from which the sets of structural parameters that deliver the transition energy or matrix element of interest may be easily read, thus allowing some optimal choice to be made.

III. NUMERICAL RESULTS AND DISCUSSION

Figure 2 shows contour plots of both the ISBT energies and dipole matrix elements squared, corresponding to the $1 \rightarrow 2$ transition in a single QW structure as functions of the relevant structural parameters [for the notation see Fig. 1(a)], i.e., the well width (l_w) and the Al content in the barrier layer ($x_b \approx U_b / \Delta E_c$, where ΔE_c is the conduction band off-

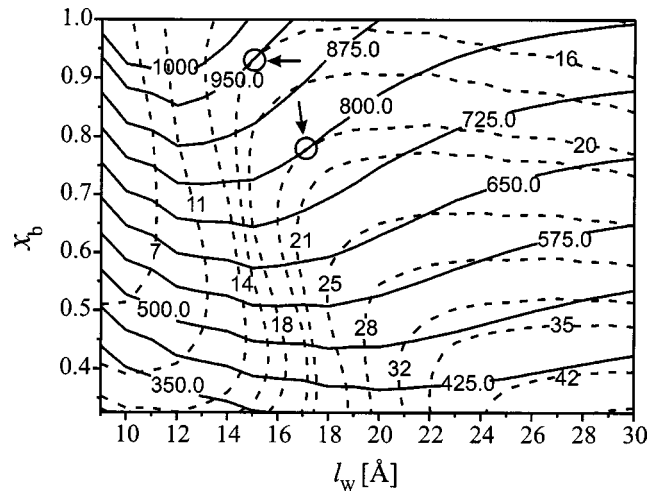


FIG. 2. Contour plot of the transition energies (solid line) and dipole matrix element squared (dashed line) between levels $|1\rangle$ and $|2\rangle$ in single AlGaIn/GaN QWs obtained for a range of structural parameters.

set set to 2 eV).^{27,28} A fixed value of the barrier width was chosen as $l_b = 60$ Å since it does not influence the results much.

In order to give specific examples, we consider the cases of 1.3 (~ 950 meV) and $1.55\mu\text{m}$ (~ 800 meV) transitions, which are important in applications. The structural parameters that deliver the $1.55\mu\text{m}$ intersubband absorption can be read from the solid line labeled 800.0 (in units of meV) in Fig. 2. Any choice along this line gives the same wavelength, but the dipole matrix element d_{12} varies. There are two sets giving, e.g., $d_{12}^2 = 16$ Å²; these are at the intersections of the dashed line labeled 16 with the 800.0 solid line. Usually one aims to have the largest possible d_{12} , and these (optimal) structural parameters occur where a dashed line just touches the 800.0 solid line: in this case it is the dashed line labeled 20, i.e., the maximal value of $d_{12}^2 = 20$ Å² and it is obtained with $l_w = 18$ Å and $x_b = 0.8$ (this point is marked by a circle and an arrow in Fig. 2). Similarly, one can see from Fig. 2 that the absorption at $1.3\mu\text{m}$ can be achieved only in a rather narrow range of parameters: $l_w \leq 17$ Å and $x_b > 0.85$, and the largest possible value of $d_{12}^2 = 16$ Å² is obtained for $l_w = 17$ Å and $x_b = 0.94$ (also marked in Fig. 2). Along with the optimal parameters, Fig. 2 shows the range of parameters that can provide any (suboptimal) structure for a given wavelength, and also indicates where the sensitivity to a parameter becomes only marginal. These may be important when the optimal design cannot be fabricated, for whatever reason.

The contour plots shown in Figs. 3 and 4 show ISBT energies corresponding to the $1 \rightarrow 2$ and $2 \rightarrow 3$ transitions in double QW structures as a function of their structural parameters [for the notation see Fig. 1(b)], i.e., the first well (l_{w1}) and middle barrier width (l_b), for two fixed values of the second well width ($l_{w2} = 6$ and 8 Å). In this calculation the outer barriers were chosen to be of AlN, in order to accommodate the three states, and their widths were also set to 60 Å. An interesting case, in view of the possible application of double QW systems as active regions of intersubband lasers, occurs when the energy of the $1 \rightarrow 2$ transition is close to the longitudinal optical (LO) phonon energy ($\hbar\omega_{\text{LO}} \approx 90$ meV in

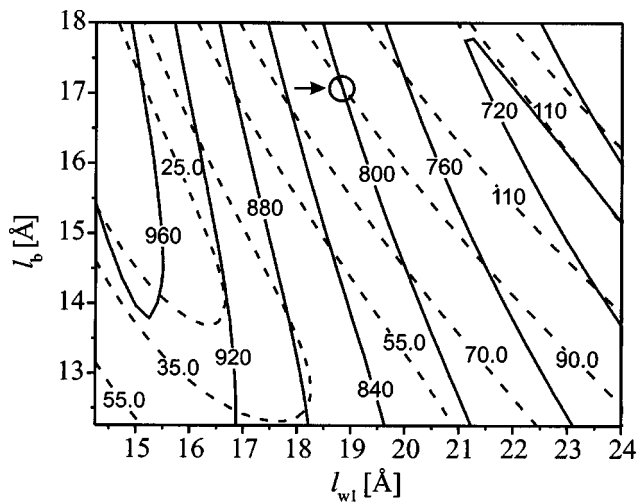


FIG. 3. Contour plot of transition energies between $|1\rangle$ and $|2\rangle$ (dashed line) and $|2\rangle$ and $|3\rangle$ (solid line) states in double AlN/GaN QWs obtained for a range of structural parameters. The second well width is set to $l_{w2} = 6 \text{ \AA}$.

GaN). This provides ultrafast depopulation of the second subband and the possibility of population inversion between levels $|3\rangle$ and $|2\rangle$. An interesting choice is if the spacing between the second and third subband is set to a wavelength of $1.55 \mu\text{m}$, which is important in fiber-based communications. For $l_{w2} = 6 \text{ \AA}$ this situation appears for the first well width of $l_{w1} = 19 \text{ \AA}$ and the middle barrier width of 17 \AA . A wider second well ($l_{w2} = 8 \text{ \AA}$) requires a much wider first well, $l_{w1} = 29 \text{ \AA}$, while the middle barrier width is $l_b = 16 \text{ \AA}$. That is a direct consequence of the presence of polarization induced fields in the layers and the therefore inherent tilt of the structure.

For any set of parameters from these diagrams, the strain-balance requirement can be straightforwardly determined from Eq. (9).

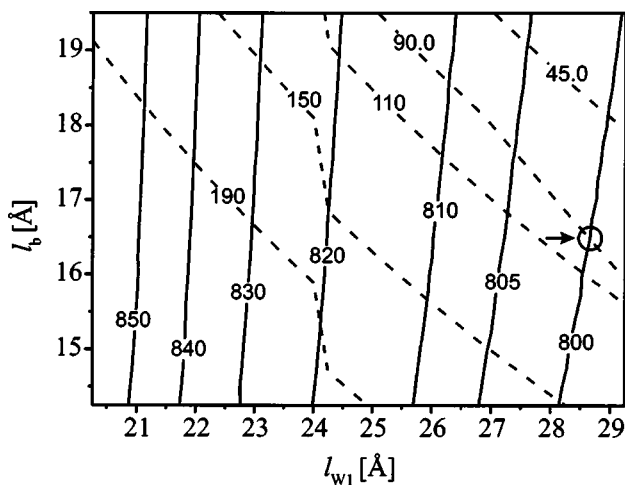


FIG. 4. Same as in Fig. 3, but for $l_{w2} = 8 \text{ \AA}$.

IV. CONCLUSION

A strain-balance condition for wurtzite GaN-based multilayer structures was been derived and useful, “design-friendly” contour plots for single and double QW structures complying with the strain-balance requirement are given. From these plots optimal parameters were extracted for ISBT absorption-based devices, as well as for a candidate structure for a three level intersubband laser.

ACKNOWLEDGMENTS

The authors would like to thank the Royal Society, EOARD and AFOSR for funding. One of the authors (V.D.J.) was supported by an ORS award.

- ¹C. Gmachl, H. M. Ng, S.-N. G. Chu, and A. Y. Cho, *Appl. Phys. Lett.* **77**, 3722 (2000).
- ²C. Gmachl, H. M. Ng, and A. Y. Cho, *Appl. Phys. Lett.* **77**, 334 (2000).
- ³C. Gmachl, H. M. Ng, and A. Y. Cho, *Appl. Phys. Lett.* **79**, 1590 (2001).
- ⁴C. Gmachl, S. V. Frolov, H. M. Ng, S.-N. G. Chu, and A. Y. Cho, *Electron. Lett.* **37**, 378 (2001).
- ⁵N. Iizuka, K. Kaneko, and N. Suzuki, *Appl. Phys. Lett.* **81**, 1803 (2002).
- ⁶K. Kishino, A. Kikuchi, H. Kanazawa, and T. Tachibana, *Appl. Phys. Lett.* **81**, 1234 (2002).
- ⁷K. Kishino, A. Kikuchi, H. Kanazawa, and T. Tachibana, *Phys. Status Solidi A* **192**, 124 (2002).
- ⁸N. Iizuka, K. Kaneko, N. Suzuki, T. Asano, S. Noda, and O. Wada, *Appl. Phys. Lett.* **77**, 648 (2000).
- ⁹J. D. Heber, C. Gmachl, H. M. Ng, and A. Y. Cho, *Appl. Phys. Lett.* **81**, 1237 (2002).
- ¹⁰H. M. Ng, C. Gmachl, S. V. Frolov, S. N. G. Chu, and A. Y. Cho, *IEE Proc.: Optoelectron.* **148**, 215 (2001).
- ¹¹A. Y. Cho, D. L. Sivco, H. M. Ng, C. Gmachl, A. Tredicucci, A. L. Hutchinson, S. N. G. Chu, and F. Capasso, *J. Cryst. Growth* **227–228**, 1 (2001).
- ¹²H. M. Ng, C. Gmachl, S. N. G. Chu, and A. Y. Cho, *J. Cryst. Growth* **220**, 432 (2000).
- ¹³N. J. Ekins-Daukes, K. Kawaguchi, and J. Zhang, *Cryst. Growth Design* **2**, 287 (2002).
- ¹⁴N. J. Ekins-Daukes *et al.*, *Sol. Energy Mater. Sol. Cells* **68**, 71 (2001).
- ¹⁵J. F. Nye, *Physical Properties of Crystals: Their Representation by Tensors and Matrices* (Oxford University Press, London, 1985).
- ¹⁶O. Ambacher *et al.*, *J. Phys.: Condens. Matter* **14**, 3399 (2002).
- ¹⁷V. Fiorentini, F. Bernardini, F. Della Sala, A. Di Carlo, and P. Lugli, *Phys. Rev. B* **60**, 8849 (1999).
- ¹⁸H. C. Liu, I. W. Cheung, A. J. Spring Thorpe, C. Dharma-Wardana, Z. R. Wasilewski, D. J. Lockwood, and G. C. Aers, *Appl. Phys. Lett.* **78**, 3580 (2001).
- ¹⁹V. Jovanović, D. Indjin, Z. Ikončić, V. Milanović, and J. Radovanović, *Solid State Commun.* **121**, 619 (2002), and references therein.
- ²⁰V. Fiorentini, F. Bernardini, and O. Ambacher, *Appl. Phys. Lett.* **80**, 1204 (2002).
- ²¹F. Bernardini and V. Fiorentini, *Appl. Surf. Sci.* **166**, 23 (2000).
- ²²F. Bernardini and V. Fiorentini, *Phys. Status Solidi B* **216**, 391 (1999).
- ²³F. Yun, M. A. Reshchikov, L. He, T. King, and H. Morkoç, *J. Appl. Phys.* **92**, 4837 (2002).
- ²⁴P. Harrison, *Quantum Wells, Wires and Dots: Theoretical and Computational Physics* (Wiley, Chichester, UK, 1999).
- ²⁵E. Sjösted and L. Nordström, *J. Phys.: Condens. Matter* **14**, 12485 (2002).
- ²⁶Fortran codes for tridiagonal matrices (after A. Rybicki) are available from <http://www.lanl.gov/DLDSTP/fast/subs.f.txt>. The code for evaluating the determinant may be simply modified to give just its sign.
- ²⁷G. Martin, A. Botchkarev, A. Agarwal A. Rockett, H. Morkoç, W. R. L. Lambrecht, and B. Segall, *Appl. Phys. Lett.* **65**, 610 (1994).
- ²⁸G. Martin, A. Botchkarev, A. Rockett, and H. Morkoç, *Appl. Phys. Lett.* **68**, 2541 (1996).